Investigating the Hydration, Mechanical Properties, and Pozzolanic Activity of Cement Paste Containing Co-Combustion Fly Ash

Xiaobo Ding [1], Hangyu Du [1], Enfeng Wu [1], Peng Yi [1], Yongqiang Li [2,*], Yaoming Luo [1] and Wei Liu [1]

[1] Guangdong Provincial Key Laboratory of Durability for Marine Civil Engineering, Key Laboratory for Resilient Infrastructures of Coastal Cities (Ministry of Education), College of Civil and Transportation Engineering, Shenzhen University, Shenzhen 518060, China; dingxb@szu.edu.cn (X.D.); 2100471021@email.szu.edu.cn (H.D.); 2200471074@email.szu.edu.cn (E.W.); 2100471026@email.szu.edu.cn (P.Y.); 2060471017@email.szu.edu.cn (Y.L.); liuwei@szu.edu.cn (W.L.)

[2] Institute of Technology for Marine Civil Engineering, Shenzhen Institute of Information Technology, 2188 Longxiang Avenue, Shenzhen 518172, China

* Correspondence: 2023000118@sziit.edu.cn

Abstract: The heat of hydration, mechanical properties, pozzolanic activity, and microscopic characteristics of cement pastes incorporating co-combusted fly ash (CCFA) were investigated, and the disparities between the CCFA/cement system and the coal fly ash (CFA) binding system were also compared. The results indicate a decrease in the heat of hydration for both CFA and CCFA samples, with a more pronounced trend observed as the fly ash content increased from 10% to 30%. The distinction in the early hydration between CFA and CCFA samples primarily manifested in the rate of heat release, potentially correlated with variations in the active Al_2O_3 content in the fly ash. Neither CFA nor CCFA samples exhibited significant cementitious activity at 3 days, functioning solely as inert fillers in the cement paste. By 3 and 28 days, the mechanical properties of both CFA and CCFA samples were inferior to those of pure cement paste. However, by 180 days of hydration, the compressive strength of CCFA-blended mortar notably increased, with the highest strength observed in the 10% CCFA-blended sample. Both CFA and CCFA samples produced the secondary hydration product C-A-S-H and demonstrated comparable consumption of calcium hydroxide (CH). These findings underscore the potential of CCFA as a supplementary cementitious material (SCM) and lay a foundation for its widespread adoption.

Keywords: co-combustion fly ash; long-term hydration; mechanical properties; microscopic characteristics; pozzolanic activity

1. Introduction

With the continuous development of urbanization, the production of sewage sludge, as the residue from municipal wastewater treatment in daily urban life, is increasing [1,2]. By 2017, the annual production of sludge in major global economies had reached approximately 38 million tons in the United States, 44 million tons in the European Union, and 55 million tons in China [3]. Projections indicate that by 2025, China's annual municipal sewage sludge production will exceed 90 million tons [4]. Notably, in the year 2022, Shenzhen, a coastal metropolis in China, generated 2.222 million tons of sludge, equating to a daily average of 6082 tons. This represented a substantial 105.2% surge in sludge production compared to levels in 2017 [5]. The swift escalation in sludge generation has intensified the urgency for responsible disposal practices. Sewage sludge is enriched with significant quantities of heavy metals, organic matter, and pathogens; thus, its direct release can impose a substantial environmental burden [1,6]. Hence, it is imperative to adopt appropriate disposal measures. Current sewage sludge disposal methods include landfill,

thermal treatment, electrochemical methods, and leaching of hazardous substances [7–10]. The use of landfill is the simplest treatment method but requires the pretreatment of fly ash to prevent environmental contamination and is constrained by land resources. Thermal treatment and leaching technologies are costly and not easily scalable, posing potential risks of secondary environmental contamination. To effectively eliminate pathogens in sewage sludge before reuse, some studies have employed combustion methods for its disposal [11,12]. The combustion of sewage sludge can be categorized into mono-combustion and co-combustion. However, sewage sludge, being a type of biomass, exhibits high ash content, volatility, and low calorific value, which makes mono-combustion uneconomical [13–15]. On the contrary, co-combustion is more widely adopted due to its lower cost and reduced environmental pollution [1,16]. For instance, Shanghai has introduced the inaugural domestic regional guidelines governing air pollutant emissions from coal-fired, integrated sludge power plants, known as DB 31/1291-2021 [17]. The enforcement of these guidelines offers a systematic foundation for addressing the air pollution challenges stemming from the co-combustion of coal and sludge.

In coal-fired power plants, the co-combustion of sewage sludge and coal results in the production of industrial by-products, namely co-combustion fly ash (CCFA) and slag, which may hold potential as supplementary cementitious materials (SCMs) for the construction industry [18–20]. Meanwhile, the cement industry accounts for about 7–8% of the global CO_2 emissions and there is an urgent need to find alternative cementitious materials such as CCFA [21]. Utilizing industrial by-products as SCMs also contributes to a higher level of circularity in the construction industry, as well as helping to reduce the depletion of natural resources. Despite its theoretical feasibility, the co-combustion of sewage sludge and coal encounters several challenges. The high levels of calcium, phosphorus, and aluminum in sewage sludge can lead to slagging and scaling issues in coal-fired boilers [22]. Moreover, due to the different sources of materials, the proportion of mineral composition in sewage sludge varies from that in coal, potentially causing combustibility problems during co-combustion [23]. For example, the desorption and combustion of volatile components within sewage sludge have a profound impact on coal combustion performance. This is attributed to the elevated volatile content present in sewage sludge, resulting in accelerated ignition and lowered ignition temperatures. As a result, the combustion process of the fuel is intensified [24,25]. The combustion properties of the fuel mixture are influenced by the combustion atmosphere and heating rate. Notably, when sewage sludge is introduced to air or oxygen-rich environments, it enhances the combustion efficiency of bituminous coal [26,27]. The positive synergistic effect of the co-combustion of sludge and coal can be attributed to the fact that certain center dot OH radicals generated by the sludge effectively disrupt the aromatic ring structure within the coal. This disruption expedites the formation of carbonaceous gases throughout the co-combustion process, leading to the observed positive effects [28]. However, the efficient removal of water content from sewage sludge through the dewatering process proves challenging, subsequently posing a hindrance to fuel combustion [29]. With the escalation in both the water content and sludge ratio, there is a gradual rise in fuel consumption coupled with a decline in boiler efficiency [30]. It has been reported that when the proportion of sewage sludge remains below 10%, the impact of moisture on combustion performance and stability of combustion products is negligible [31].

The utilization of by-products from sewage sludge incineration is still limited due to concerns regarding the containing of significant amounts of heavy metals and dioxins, which can contaminate the environment [32,33]. In addition, a high proportion of sewage sludge co-combustion with fuel leads to heightened emissions of sulfur and nitrogen oxides, which subsequently escalates the expenses associated with the removal of these detrimental constituents from the flue gas [34]. In an analysis encompassing the mass balance and distribution characteristics of heavy metals and dioxins throughout the co-combustion process, it was determined that maintaining the sewage sludge blend below 20% resulted in emissions falling below the prescribed standard limits [13]. Similarly,

leaching tests performed across different nations have demonstrated that a sewage sludge ratio below 25% effectively controls the leaching of hazardous phases, thereby establishing the environmentally friendly nature of utilizing CCFA [35]. Based on the findings from these investigations, it is crucial to strictly limit the proportion of sewage sludge co-fired with coal to meet the basic environmental and construction industry requirements. So far, the influence of coal fly ash (CFA) on cement properties has been extensively investigated, and it has become a widely used mineral admixture in cement [36–39]. However, research on the use of CCFA in cementitious systems remains limited, as its properties are not yet fully comprehended. Therefore, it is essential to conduct systematic studies on CCFA to explore its potential as SCMs.

To examine the suitability and properties of CCFA with sewage sludge as a sustainable replacement for ordinary Portland cement, this investigation delves into the effects of CFA and CCFA sourced from Shenzhen on cement paste, focusing on the hydration process, mechanical properties, and pozzolanic activity. The suitability of CCFA as an SCM for cement production was assessed. Isothermal calorimetry was employed to analyze the early hydration characteristics of CFA and CCFA samples. Subsequently, changes in compressive strength were utilized to evaluate the pozzolanic activity of both types of fly ash. The microstructures and hydration products of both CFA and CCFA samples underwent examination via scanning electron microscopy (SEM), X-ray diffraction (XRD), and thermogravimetric analysis (TGA) to ascertain their analogous micro characteristics and long-term activities. These findings underscore the potential of CCFA as an SCM and lay a foundation for its widespread adoption.

2. Materials and Test Methods

2.1. Raw Materials

Prior to studying CCFA, an assessment of the fundamental properties of the sewage sludge (SS) was performed. The selected SS was obtained from a sewage treatment plant in Shenzhen, China, as illustrated in Figure 1a. The basic characteristics of SS are shown in Table 1. As indicated in Table 1, it is revealed that SS possesses a low calorific value, which may lead to increased energy consumption when burned alone. For better combustion, only 10% of SS was chosen for co-combustion with coal in this study. Table 2 shows that the top four ranked oxides of SS are SiO_2, Al_2O_3, Fe_2O_3, and P_2O_5.

Figure 1. Morphologies of raw materials: (**a**) sewage sludge; (**b**) CFA; and (**c**) CCFA.

Table 1. Basic characteristics of sewage sludge.

Characterization	Value	Standard Limit
High/low calorific value of dry basis (MJ/kg)	7.91/7.2	
High/low calorific value on wet basis (MJ/kg)	6.28/5.3	
Received base volatile (wt. %)	27.19	
Received base fixed carbon (wt. %)	3.86	
Received base ash (wt. %)	48.36	None
Organic matter (wt. %)	42.41	
Full moisture (wt. %)	20.59	
Total number of bacteria (count /g)	1.7×10^4	

Table 1. *Cont.*

Characterization	Value	Standard Limit
Ascaris egg mortality (%)	100	$\geq$95 [38]
Fecal coliform value	>11.1	$\geq$0.01 [38]

Note: none refers to no limit found in the standard.

Table 2. Chemical composition of raw materials (wt. %).

Name	SiO$_2$	Al$_2$O$_3$	Fe$_2$O$_3$	CaO	P$_2$O$_5$	K$_2$O	MgO	SO$_3$	Na$_2$O	Others
SS	48.18	24.08	15.22	1.08	6.17	2.35	0.90	0.05	0.48	1.49
OPC	22.37	4.36	3.38	61.08	-	-	2.43	2.45	-	3.93
CFA	44.31	20.50	9.16	15.31	0.32	1.21	1.99	1.59	3.81	1.80
CCFA	46.56	30.66	7.50	7.46	1.54	1.32	1.23	0.99	1.02	1.72

The ordinary Portland cement (OPC) used in this experiment was produced by the China United Cement Company, in accordance with the specifications of GB 8076-2008 [40]. The oxide composition and basic properties of the OPC are shown in Tables 2 and 3. The selected CFA (Figure 1b) and CCFA (Figure 1c) were both derived from the Mawan coal-fired power plant in Shenzhen, China. The co-combustion process for producing CCFA is briefly illustrated in Figure 2, comprising 10% sewage and 90% coal being blended in a mixing system, followed with a milling process in a milling system. Subsequently, the blended and milled particles were put into the combustion system for co-combustion, and the combusted CCFA was collected through an electrostatic precipitator from the flue. For stability assessment, one batch of CCFA was collected from the power plant each month, and six batches in total were collected.

Table 3. Basic properties of OPC.

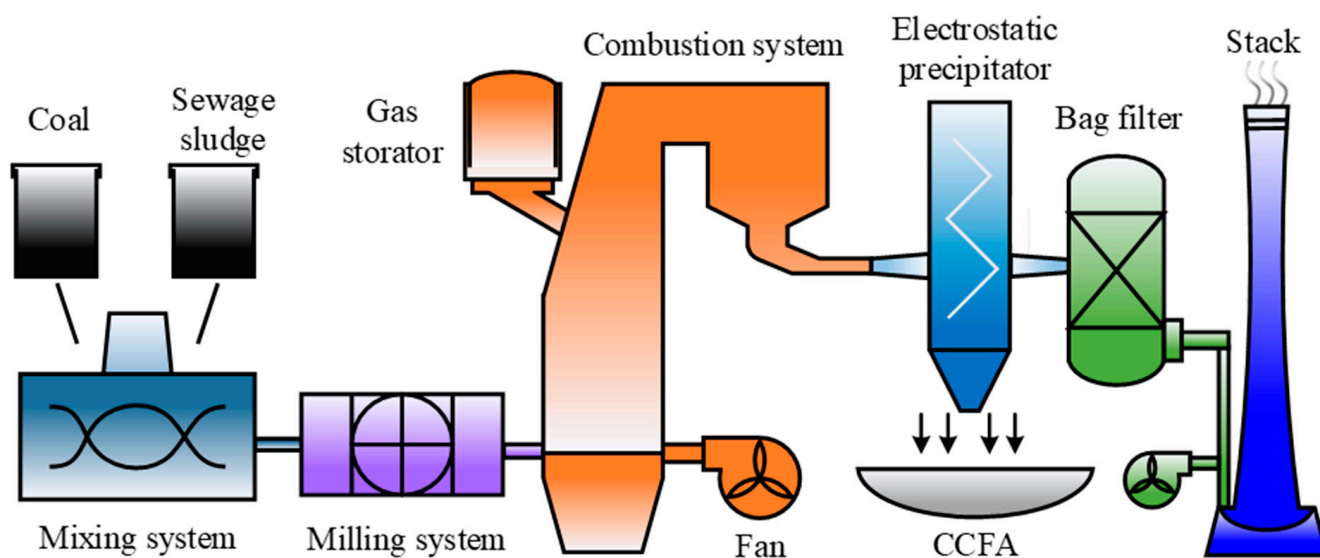| Density/(g/cm^3)	Specific Area/(m^2/kg)	Compressive Strength/MPa		Flexural Strength/MPa	
		3 d	28 d	3 d	28 d
3.15	340	28.4	48.2	6.0	8.7

Figure 2. Sewage sludge and coal co-combustion process.

The particle size distribution of fly ashes, analyzed using a laser particle size analyzer, is illustrated in Figure 3. The median particle sizes of CFA and CCFA are 10.52 µm and 18.15 µm, respectively, indicating that selected CCFA has coarser particles compared to CFA. The chemical compositions of two fly ashes, determined by X-ray fluorescence spectrometric analysis, are presented in Table 3. Both fly ashes are primarily composed of SiO_2, Al_2O_3, and CaO. However, the CCFA exhibited higher levels of Al_2O_3 and P_2O_5 compared to CFA, which can be attributed to the incorporation of SS.
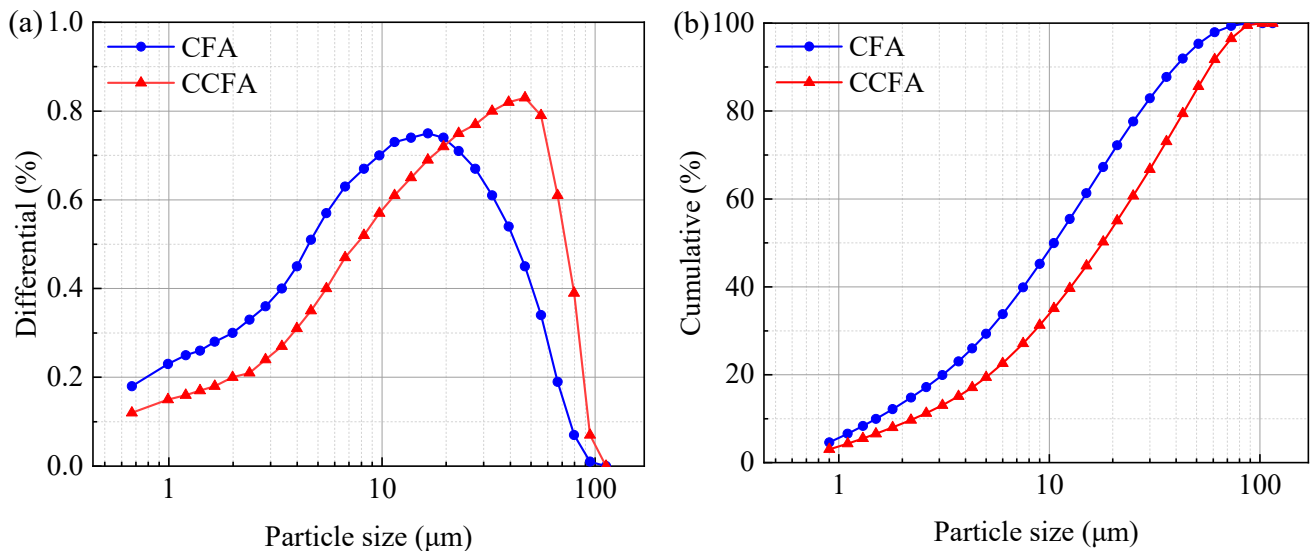
Figure 3. Particle size distribution of fly ashes with (**a**) differential and (**b**) cumulative curves.

2.2. Sample Preparation

In this experiment, a water–cement ratio of 0.5 was employed, and deionized water was used as the mixing water. Seven paste samples with various mixing ratios were designed and are listed in Table 4. The pure cement paste used as the reference sample is labeled as REF. The blended pastes were named as CFA1, CFA2, CFA3, CCFA1, CCFA2, and CCFA3 based on the replacing proportion of CFA and CCFA to cement from 10% to 30%. The freshly mixed paste was poured into a sealed plastic tube (R = 10 mm × H = 100 mm), fixed on a rotary mixer, and rotated at 10 r/min for 24 h to prevent sample separation. Subsequently, the plastic tubes were cured under the sealed conditions at 22 ± 2 °C. After 28 and 180 days of curing, the samples were demolded to stop hydration for microscopic measurements following the procedure outlined in reference [41].

For mechanical testing, mortar specimens with dimensions of 40 × 40 × 160 mm and a cement–sand ratio of 1:3 were cast following the guidelines specified in GB/T 17671 [42]. After 3, 28, and 180 days of curing, the compressive and flexural strength were tested, respectively. A sketch of all the experiments is shown in Figure 4.

Table 4. Mixture details for cement pastes.

Name	*w/c*	Cement (g)	CFA (g)	CCFA (g)	Water (g)
REF	0.5	450	0	0	225
CFA1	0.5	405	45	0	225
CFA2	0.5	360	90	0	225
CFA3	0.5	315	135	0	225
CCFA1	0.5	405	0	45	225
CCFA2	0.5	360	0	90	225
CCFA3	0.5	315	0	135	225
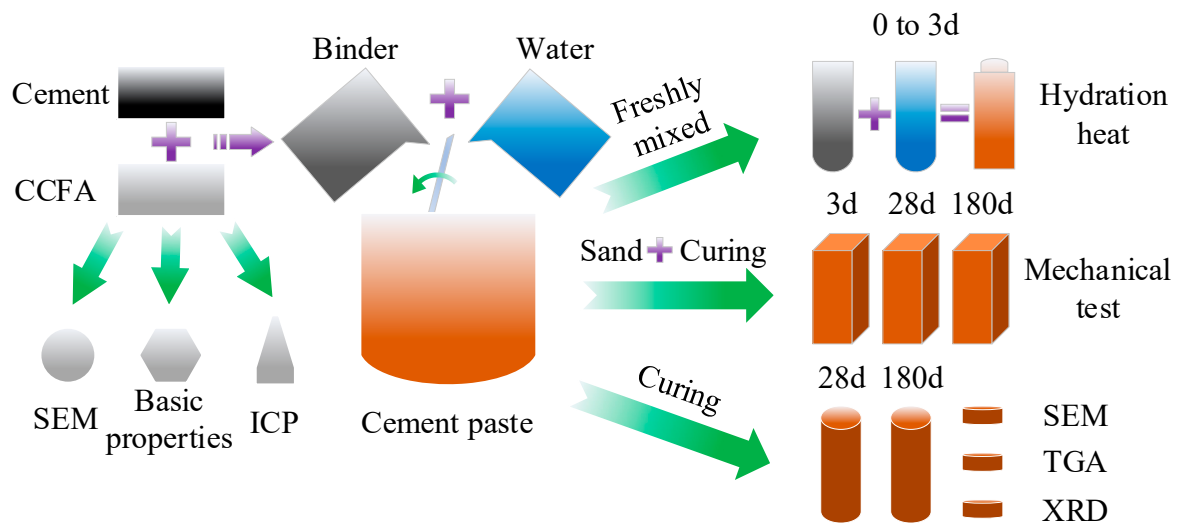
Figure 4. Sketch of the experimental process.

2.3. Test Methods

2.3.1. Isothermal Calorimetry

The hydration process of fly ash-blended cement paste was monitored using an isothermal calorimeter (TAM Air; TA Instruments, New Castle, DE, USA). The total sample mass was precisely weighed as 3 ± 0.0001 g. All raw materials were combined in a glass vial and mixed thoroughly on a vibrator. The heat release rate and the accumulated heat release were recorded continuously for 72 h.

2.3.2. Mechanical Properties and PEC

The mechanical properties were assessed using an integrated cement flexural and compressive test machine (TJSK-300S; Tianjin Shenke Testing Instrument Co., Tianjin, China). To evaluate the pozzolanic activity, the pozzolan effectiveness coefficient (PEC) was defined as Equation (1) [43].

$$\mathrm{PEC} = \frac{f_c(\mathrm{Px}) - (1 - \mathrm{x}/100) f_c(\mathrm{R})}{f_c(\mathrm{R}) \cdot \mathrm{x}/100} \tag{1}$$

where $f_c(\mathrm{Px})$ and $f_c(\mathrm{R})$ (MPa) are the compressive strength of fly ash-blended paste and REF, respectively; and x (%) is the replacing ratio of fly ash.

The PEC result is evaluated based on the following principles [43]: (i) PEC < 0: the material is regarded as a filler without any pozzolanic activity; (ii) 0 < PEC < 1: the applied admixture is considered to possess pozzolanic activity, with higher PEC values indicating higher pozzolanic activity; (iii) PEC > 1: the pozzolanic activity is more effective than that of cement, suggesting a synergistic cement–pozzolan–water system.

2.3.3. SEM-EDS

The microscopic morphology was observed with a ZEISS Gemini SEM equipped with energy dispersive spectroscopy (EDS). The cement paste was gently cracked with a hammer, and a small sample was extracted after the hydration process was terminated. The sample was then dried in a vacuum drying oven at 40 °C for 24 h. Before measurement, a thin layer of gold was sprayed on the sample surface to ensure good electrical conductivity.

2.3.4. XRD

The hydration-terminated samples were ground into powder and then passed through an 80 μm sieve. Measurements were carried out using a D8 Advance diffractometer from Bruker, Germany, with a scanning interval of 5–70° 2θ and scanning step of 0.02°/s.

Quantitative XRD was used to calculate the content of amorphous phase content in fly ash, with an external standard of zinc oxide. High Score Plus software V3.0.5 was employed for data analysis.

2.3.5. TG-DTG

The same batch of samples utilized for XRD analysis were also subjected to TGA analysis. The test equipment was SQT-Q600 from TA, New Castle, DE, USA, with a temperature range of 30–800 °C and a heating rate of 10 °C/min under a nitrogen environment. The content of calcium hydroxide was calculated based on the mass loss, as described in Equation (2).

$$Ca(OH)_{2,measured} = \frac{WL_{Ca(OH)_2}}{m_{800}} \times \frac{m_{Ca(OH)_2}}{m_{H_2O}} \qquad (2)$$

where $WL_{Ca(OH)_2}$ (%) is the mass loss due to the decomposition of calcium hydroxide in the range of 350–550 °C; m_{800} refers to the mass residue at 800 °C; $m_{Ca(OH)_2}$ and m_{H_2O} are the molar mass of calcium hydroxide and water, 74 g/mol and 18 g/mol, respectively.

3. Results and Discussion

3.1. Basic Properties and Variability of CCFA

The micro-morphologies of the two fly ashes are depicted in Figure 5. Generally, CCFA has a similar micro-morphology to CFA. The incorporation of sewage sludge in CCFA results in a reduction in the number of spherical particles and an increase in irregular particles when compared to CFA. A similar phenomenon was also observed by Piasta et al. [44]. Consequently, CCFA displays a larger median particle size than CFA (Figure 3).
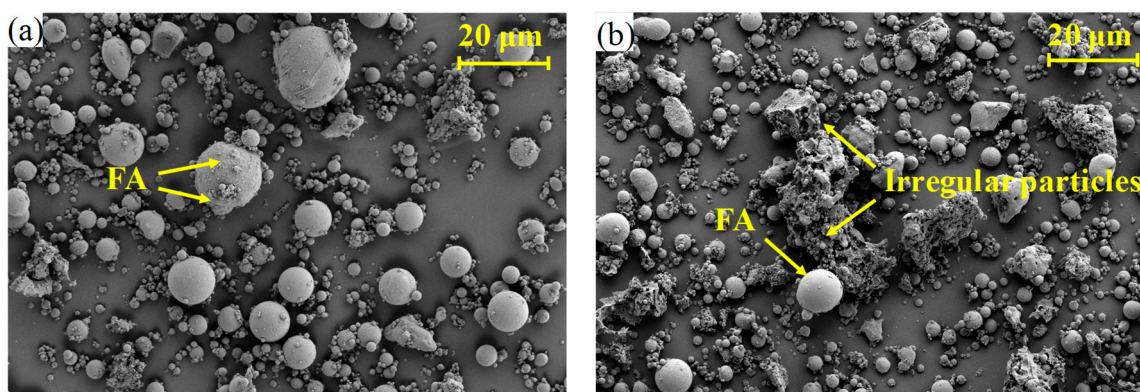

Figure 5. SEM images of two types of fly ash: (**a**) CFA and (**b**) CCFA.

The physical and chemical properties of six batches of CCFA were measured in accordance with the standard GB/T 1596-2017 [45]. A total of 24 samples (four samples × six batches) were analyzed, and the results are presented in Table 5. The indicators examined include water content, water demand ratio, fineness, stability, ignition loss, and mass fraction of SO_3. The results show that all of the tested parameters meet the standard requirements in [45], indicating that CCFA has potential for engineering applications.

Table 5. Physical and chemical properties of six batches of CCFA.

| Physical and Chemical Properties	Range of Fluctuations	Standard Limit [44]
Water content (%)	0.1–0.2	≤1.0
Water demand ratio (%)	90–98	≤105
Fineness (45 μm) (%)	3.1–25.6	≤30.0
Stability (mm)	0–1.5	≤5.0
Ignition loss (%)	0.61–2.15	≤8.0
Mass fraction of SO_3 (%)	0.28–1.07	≤3.0

The XRD patterns are shown in Figure 6a. The primary crystalline components of CCFA and CFA are quartz (SiO_2) and mullite ($Al_6Si_2O_{13}$), whilst small amounts of hematite (Fe_2O_3) are also observed. The quantitative result is shown in Figure 6b. It is found that CCFA contains a smaller amorphous phase and more mullite compared to CFA. This can be attributed to the fact that as the particle size of fly ash decreases, the conversion rate of molten crystals to the amorphous phases is accelerated [46]. Given that the average particle size of CCFA is larger than that of CFA (see Figure 3), fewer amorphous phases are formed during the cooling process. Moreover, the slow movement of the melted large particles in CCFA facilitates the recrystallization of mullite, leading to an increased crystal content.
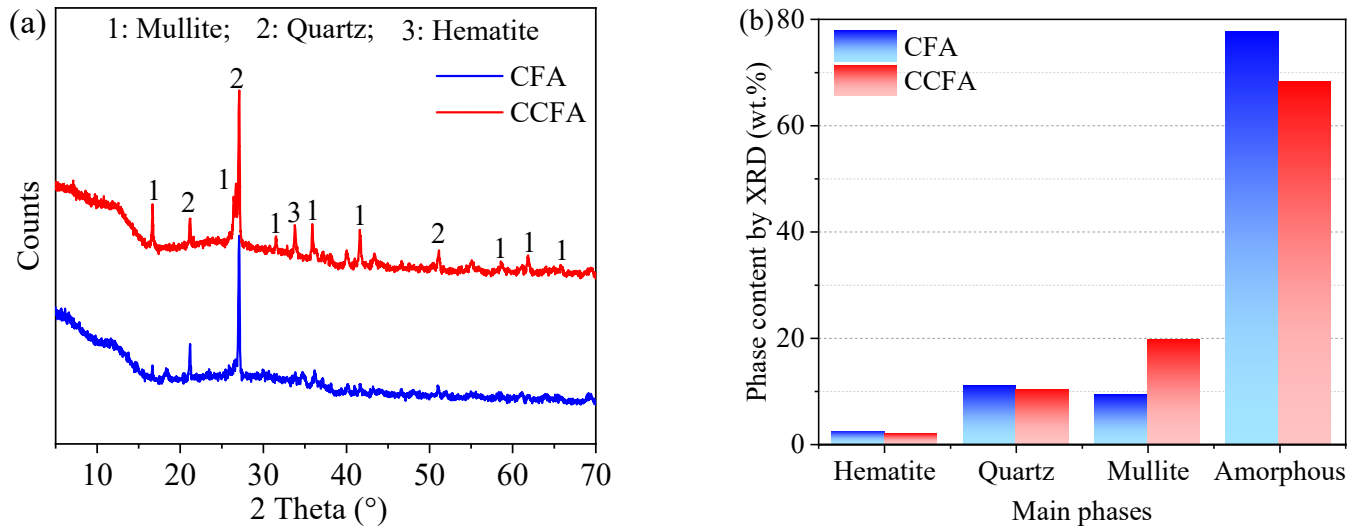
Figure 6. XRD patterns of fly ashes: (**a**) main phase composition and (**b**) quantitative results.

3.2. Hydration Performance of SCMs

The results of the hydration heat are presented in Figures 7 and 8, with the data normalized to the mass of cementitious material. Following the classical isothermal calorimetric curve of cement [47–49], the hydration process can be divided into four stages: initial, induction, acceleration, and deceleration stages.
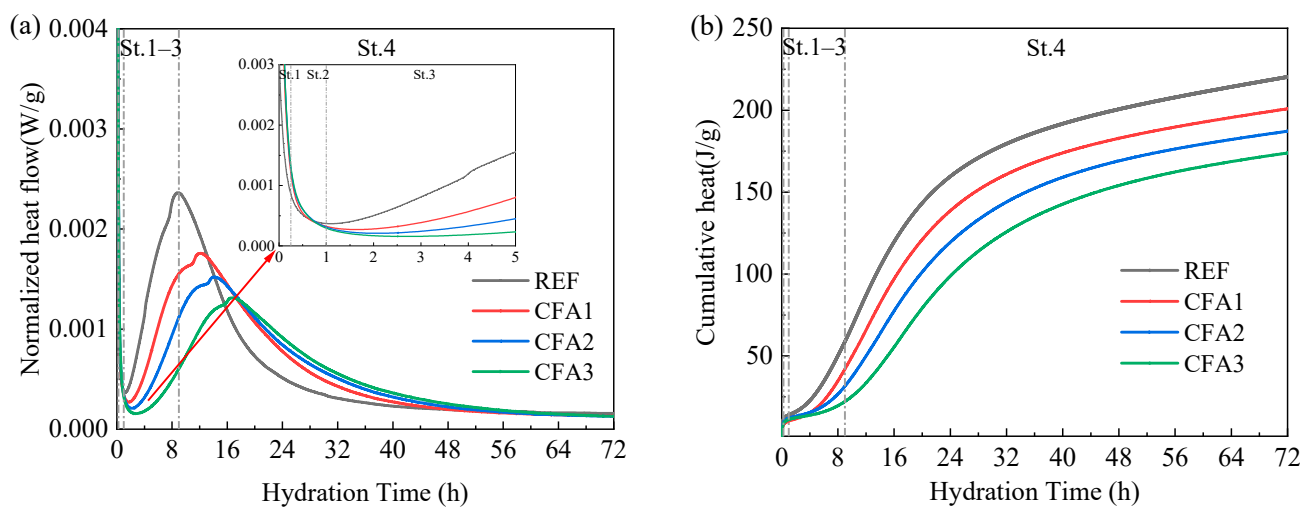
Figure 7. (**a**) Heat release rate and (**b**) cumulative heat release for CFA-blended cement pastes.
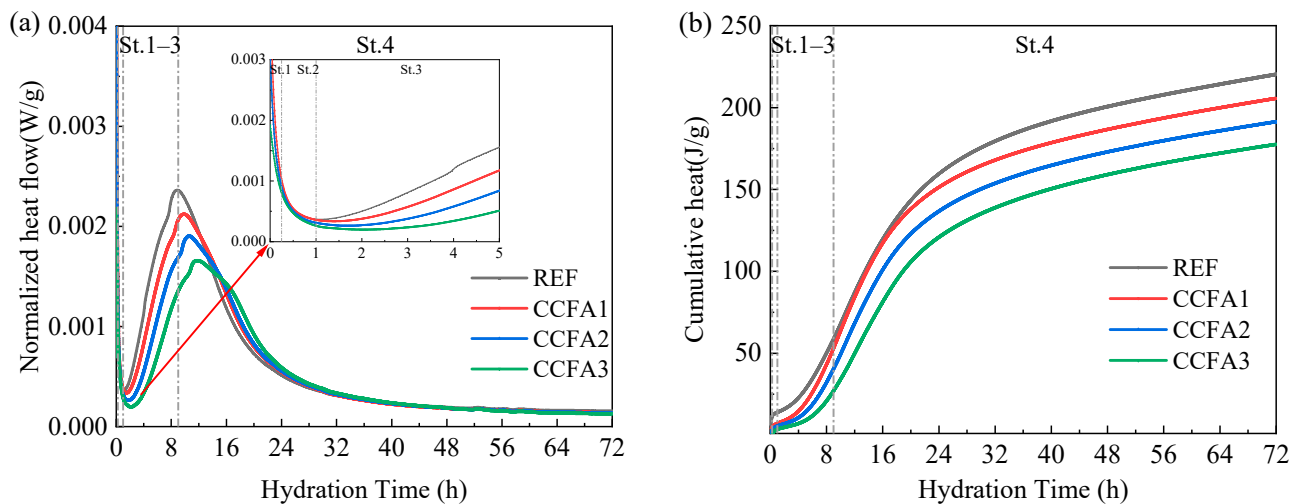
Figure 8. (**a**) Heat release rate and (**b**) cumulative heat release for CCFA-blended cement pastes.

Upon continuous contact between water and cement, the hydration reaction commences immediately. The dissolution of active minerals such as C_3A leads to the first exothermic peak [47]. During the initial stage (St. 1), no significant differences in the cumulative heat release between CCFA and CFA samples were observed.

The heat release rate remained at a low and steady state during the induction stage (St. 2). The increase in the blending ratio of CFA and CCFA was found to extend the duration of the induction stage. This phenomenon can be attributed to the low calcium–silica specific surface of fly ash, which can adsorb Ca^{2+} from the solution. This adsorption process inhibits the nucleation and crystallization of calcium hydroxide (CH) and calcium silicate hydrate (C-S-H), consequently retarding the overall hydration process [50–52]. Furthermore, the induction period of CCFA samples was observed to be shorter than that of CFA samples when using the same admixture. In comparison to the REF's end of 1 h, CCFA1, CCFA2, and CCFA3 had ends of approximately 1.41 h, 2 h, and 2.5 h, whereas CFA1, CFA2, and CFA3 lasted approximately 2 h, 2.5 h, and 3.3 h, respectively. The observed difference should be related to the formation of active Al_2O_3 compounds in CCFA during the combustion of pozzolan additives [53]. CCFA contains a higher alumina content than CFA (refer to Table 3), which allows CCFA samples to release more aluminate ions compared to CFA samples. As a result, the consumption of gypsum is accelerated, leading to a faster hydration rate in CCFA samples.

Entering the acceleration stage (St. 3), a rapid increase in the heat release rate is observed. The REF displayed two exothermic peaks at approximately 8.4 h and 10.7 h, which were attributed to the hydration of silicate and the depletion of sulfate, respectively [47,54]. However, upon partial replacement of cement by fly ash, the available amount of clinker for the hydration reaction decreased. Consequently, the exothermic peaks of samples containing CFA and CCFA were observed at later times compared to the REF. Moreover, as the fly ash admixture increased, the cumulative heat release decreased [51]. For the identical admixture, the exothermic rate and cumulative exothermic amount of CCFA samples surpassed those of CFA samples by a slight margin. This phenomenon may stem from the higher presence of irregularities and impurities in CCFA compared to CFA (refer to Figure 5), thereby offering supplementary attachment sites for hydration reactions [55].

During the deceleration stage (St. 4), the exothermic rate starts to decrease to low values. A shoulder peak also becomes evident within the time range of approximately 16 h to 22 h when the CCFA blending exceeds 10%. This observation may be the result of the early local pozzolanic reaction [56]. At 72 h, the cumulative heat release of samples was found to be nearly identical for the same mixture of CFA and CCFA.

Generally, CFA and CCFA samples reduce the maximum heat flow, which is beneficial for massive concrete structures as the risk of thermal heat cracks may be reduced [57]. The

primary difference lies in the early hydration rate, which is determined by the fundamental properties of the raw materials.

### 3.3. Mechanical Properties and Pozzolanic Activity of SCMs

The long-term mechanical properties of mortars containing different blending ratios of CFA and CCFA are illustrated in Figure 9. At 3 d and 28 d, the strengths of both CFA and CCFA samples were lower than the REF, and kept in decreasing tendency with increasing blends. It can be explained that fly ash replaces a portion of the cement to result in a reduced hydration degree and make the early strength grow slow [58,59]. As the curing age increased, the secondary hydration reaction of fly ash took place, gradually exhibiting pozzolanic activity [55,60]. By 180 d, the strength of CCFA and CFA samples had increased significantly. The products of pozzolanic reactions, such as C-S-H and C-A-S-H, contributed to a capillary filling effect, which densified the microstructure and enhanced the overall strength of the system [61]. The compressive strength of CFA1, CFA2, and CCFA1 surpassed that of the REF, whilst only the flexural strength of CCFA1 exceeded the REF.
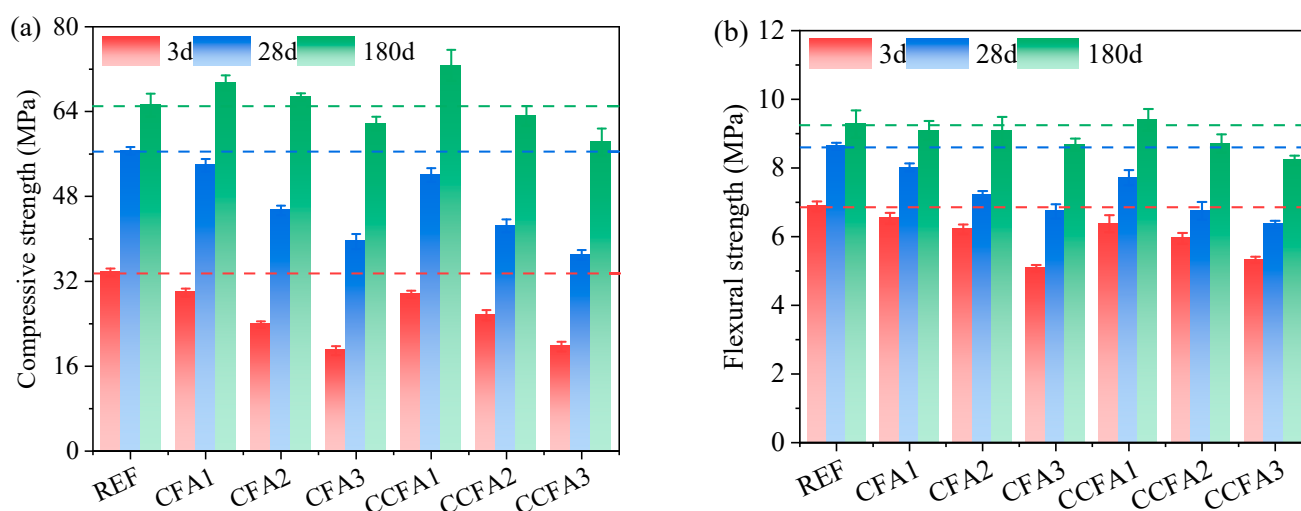
Figure 9. Mechanical properties of fly ash-blended mortar after 3, 28, and 180 days of hydration: (**a**) compressive strength and (**b**) flexural strength.

The PEC, calculated using Equation (1), provides further insight into the pozzolanic activity, as depicted in Figure 10. At 3 d, all mortars containing blended fly ash had PEC < 0, indicating a lack of pozzolanic activity during the early hydration period. Instead, the fly ashes behaved as inert fillers at this stage. However, at 28 days, both CFA1 and CCFA1 samples showed positive PEC values, demonstrating the onset of pozzolanic activity in these mixtures. At 180 d, all fly ash-blended samples exhibited significant pozzolanic activity (PEC > 0.5). Specifically, the strength and PEC of CCFA1 at 180 d were the highest among the samples, indicating the best synergistic effect of CCFA with cement at 10% blending ratio. This finding demonstrates that incorporating CCFA at a modest blending proportion can notably improve the long-term compressive strength as well as the pozzolanic reactivity of the cementitious system.

In general, incorporating both CCFA and CFA into the cement improved the long-term mechanical properties; the 10% blending ratio is the optimal replacing ratio for CCFA.
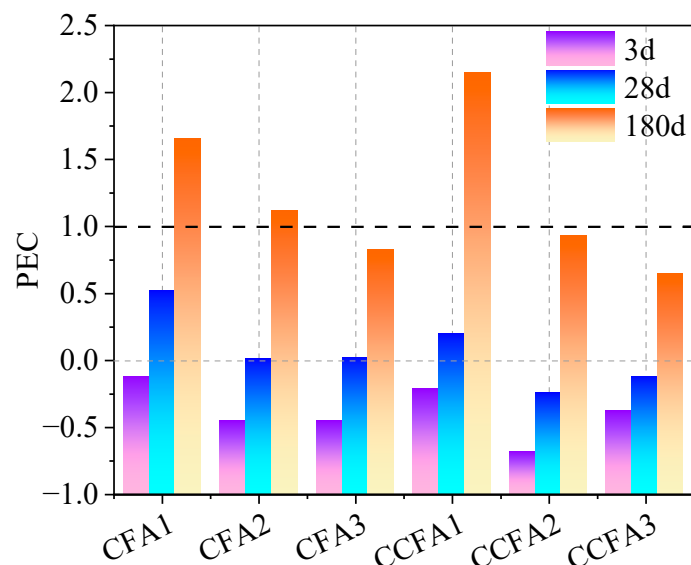
Figure 10. PEC values of fly ash-blended mortar after 3, 28, and 180 days of hydration.

### 3.4. Microscopic Characteristics of SCMs

3.4.1. SEM-EDS Analysis

SEM and EDS results for cement pastes curing after 28 and 180 days are displayed in Figures 11 and 12, respectively. At 28 d, typical hydration products such as AFt and C-S-H were observed in the REF. At this time, the CFA sample and CCFA sample were loosely packed with hydration products around the fly ash particles (Figure 11b,c). The morphology of the fly ash was easily distinguishable, with no apparent secondary hydration features, suggesting that the pozzolanic reaction was not yet obvious at this early stage. However, at 180 d, the microstructure became dense as hydration continued. The C-S-H in the REF transformed from a coarse network to a compact cluster [62–64]. Additionally, a dense layer of hydration products was observed on the fly ash surface (Figure 11e,f), indicating that the pozzolanic reaction had progressed sufficiently by this time. The reactive SiO_2 and Al_2O_3 in the fly ash reacted with CH in the cement paste to form C-A-S-H, which aggregates on the fly ash surface [65]. Inside the CCFA samples, the irregularly shaped CCFA particles had integrated with the hydration products and were difficult to distinguish from each other.

Based on the EDS results (see Figure 12), the proportion of elemental Al in fly ash-blended cement pastes increases with age, confirming that this hydration product is C-A-S-H. The presence of C-A-S-H serves as evidence for the occurrence of secondary hydration reactions [54,66]. Furthermore, the Ca/Si ratio of C-S-H in REF increased from 1.92 (Figure 12a) to 2.26 (Figure 12d). Conversely, the Ca/Si ratios of C-A-S-H around both fly ashes exhibited a decreasing trend, from 1.41 (Figure 12b) to 1.06 for CFA3 (Figure 12e), and from 1.58 (Figure 12c) to 1.01 (Figure 12f) for CCFA3.

In summary, the SEM-EDS results confirmed that CCFA and CFA samples have similar microscopic morphology and hydration products. At 28 days, CCFA3 and CFA3 primarily acted as fillers, with limited evidence of secondary hydration. However, at 180 days, the presence of C-A-S-H indicated significant secondary hydration, leading to enhanced mechanical properties of the cement paste, aligning with the PEC results (Figure 10).
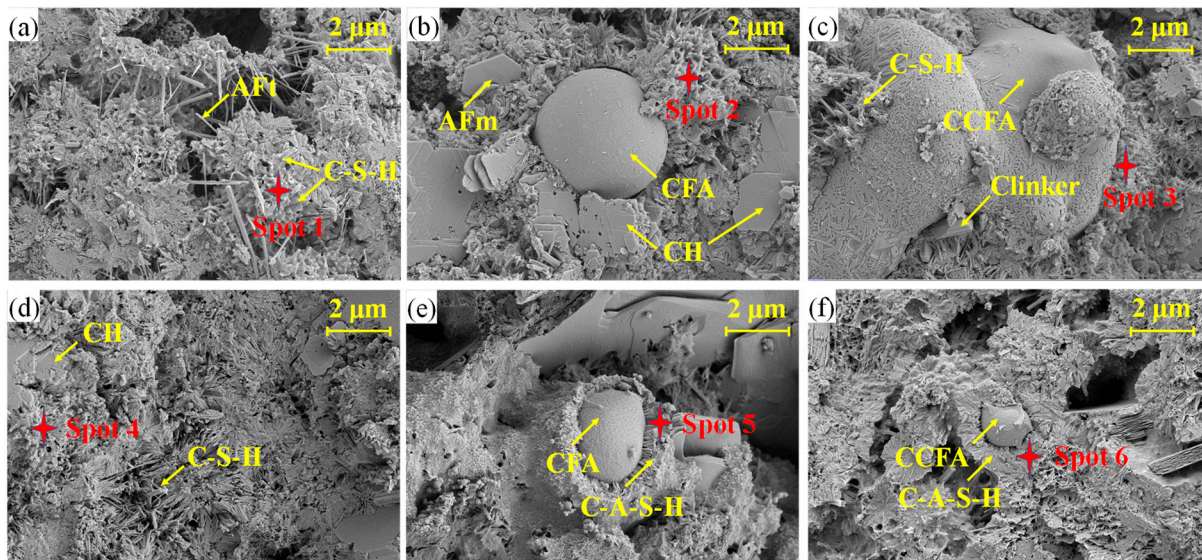
Figure 11. Microscopic morphology of fly ash-blended cement pastes at different ages: (**a**) REF hydrated for 28 d; (**b**) CFA3 hydrated for 28 d; (**c**) CCFA3 hydrated for 28 d; (**d**) REF hydrated for 180 d; (**e**) CFA3 hydrated for 180 d; (**f**) CCFA3 hydrated for 180 d.
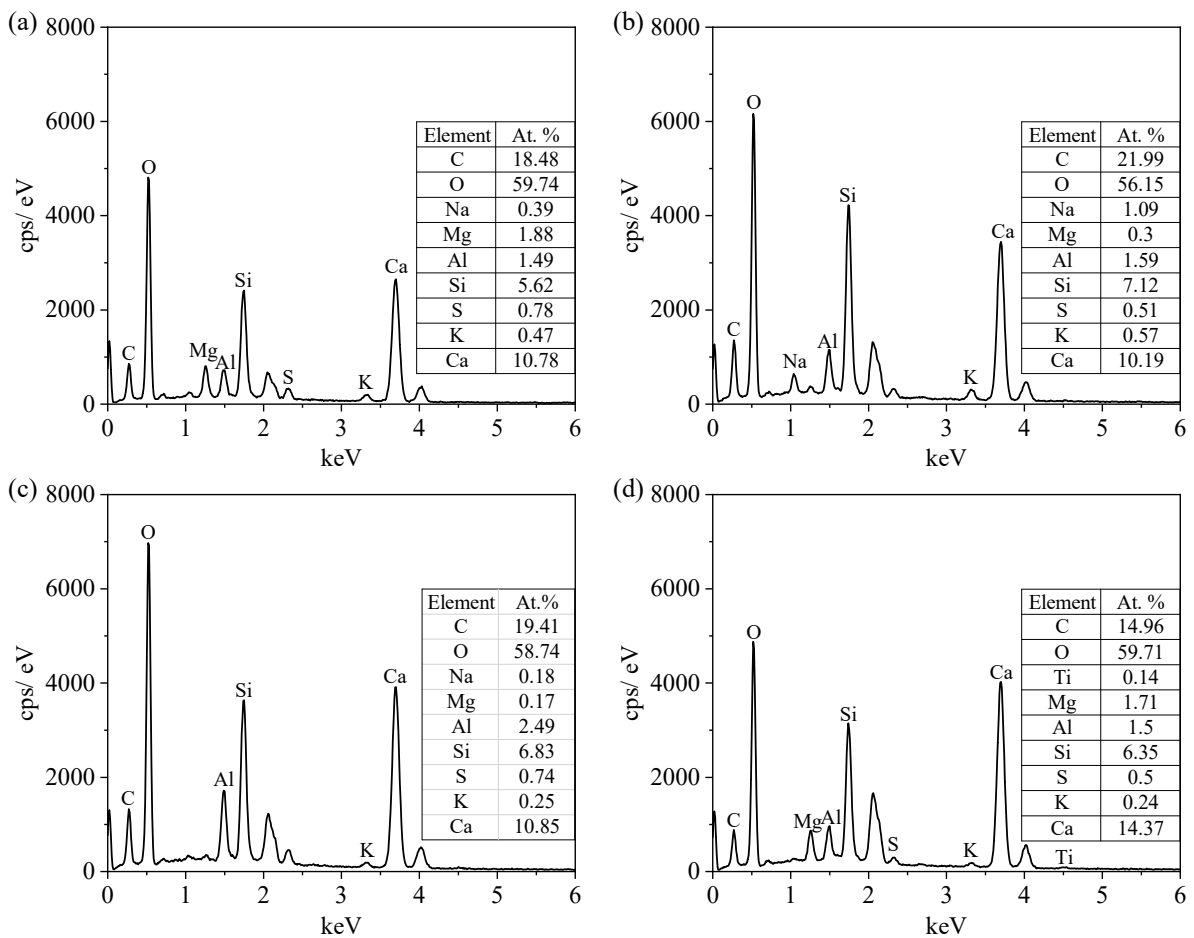

Figure 12. *Cont*.
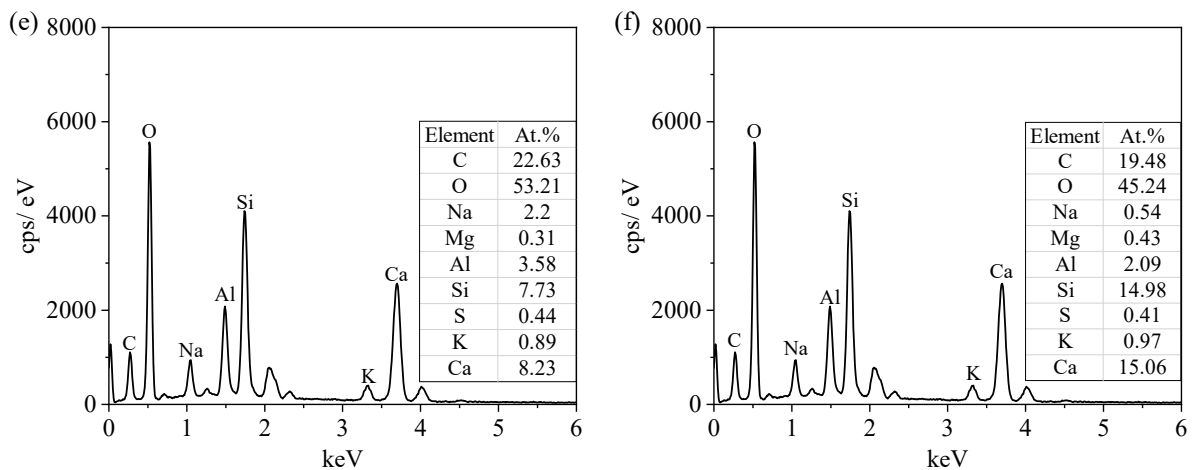
Figure 12. SEM-EDS patterns of fly ash-blended cement pastes at 28 d and 180 d: (**a**) Spot1; (**b**) Spot2; (**c**) Spot3; (**d**) Spot4; (**e**) Spot5; (**f**) Spot6.

3.4.2. XRD Analysis

Figure 13 shows the XRD patterns of cement pastes at 28 and 180 days. The major crystalline components of CCFA3 and CFA3 include portlandite (CH), ettringite (AFt), and monosulfate (AFm). Compared to REF, both CFA3 and CCFA3 exhibit an additional peak of quartz, which is introduced by the presence of fly ash (Figure 6). At 28 days, the intensity of the CH peaks in CFA3 and CCFA3 was lower than that of the REF. According to the results of PEC (Figure 10) and SEM (Figure 11), at this time, the two types of fly ash had not yet exhibited pozzolanic activity. Consequently, the above phenomenon is due to the replacing of cement by the fly ash, leading to the decrease in CH generation. As the hydration time increased, the intensity of the CH peak of CCFA3 and CFA3 visibly reduced, signifying the occurrence of pozzolanic reactions. At 180 d, the XRD curves of CFA3 and CCFA3 nearly overlapped, indicating that the composition of the major phases of the two fly ashes are similar.

In conclusion, the XRD findings, together with the SEM-EDS results, provide strong evidence that both CCFA and CFA samples possess comparable long-term hydration properties and mineral compositions.
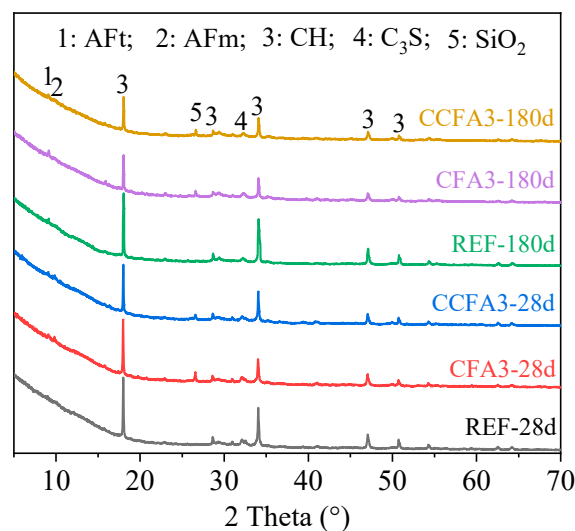
Figure 13. XRD patterns of fly ash-blended cement pastes at 28 d and 180 d.

3.4.3. TG-DTG Analysis

Figure 14 presents the TGA curves of CFA and CCFA-blended cement paste after 28 and 180 days of hydration. The initial weight loss observed in the temperature range of 30–200 °C is attributed to the decomposition of C-S-H, AFt, and AFm [67]. The second weight loss peak, observed in the range of 350–550 °C, corresponds to the decomposition of CH. The fly ash activity can be assessed based on the relative mass change in CH [68], as depicted in Figure 15. At 28 days, the CH contents in CFA3, CCFA3, and REF were 18.8%, 19.3%, and 23.2%, respectively. After 180 days, the CH content in REF increased to 27.5%, while in CFA3 and CCFA3, it decreased to 15.6% and 16.5%, respectively, due to the depletion of pozzolanic reactions [69,70]. These findings are consistent with the XRD results.

The TGA analysis provided further insights into the pozzolanic activity of CCFA and CFA samples. The closely similar CH contents in CFA3 and CCFA3 suggest that both materials exhibit comparable long-term pozzolanic activity. The TGA analysis revealed that the CH contents in CFA3 and CCFA3 were quite similar, indicating that CCFA and CFA samples exhibit comparable pozzolanic activity.
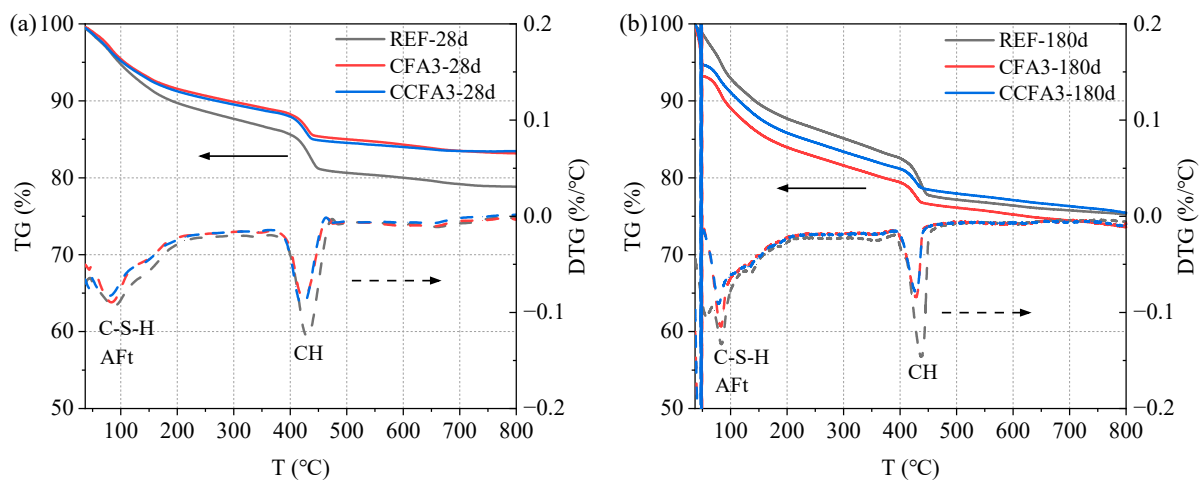

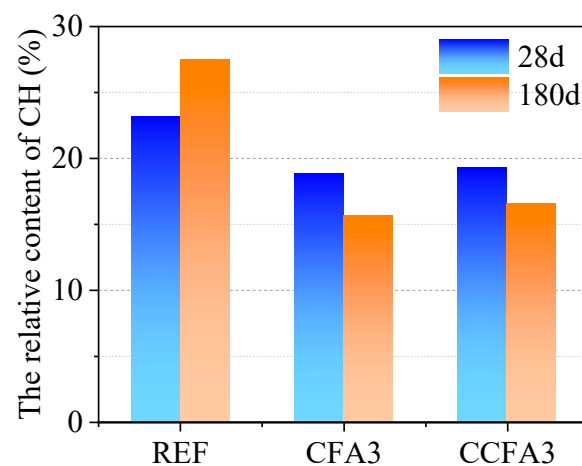**Figure 14.** TG-DTG curves of fly ash-blended cement pastes: (**a**) 28 d and (**b**) 180 d.

Figure 15. CH content of fly ash-blended cement pastes (relative to mass residue at 800 °C).

4. Conclusions

In this paper, the fundamental properties of co-combustion fly ash (CCFA) were characterized. Subsequently, the feasibility of CCFA as supplementary cementitious materials (SCMs) was explored, using a series of assessments including isothermal calorimetry, me-

chanical properties, pozzolanic activity, and microscopic morphology. The main research results are summarized as follows:

(1) CCFA and CFA are similar in terms of major mineral composition. Compared with CFA, CCFA has more mullite and less amorphous phase. The physical and chemical properties of all batches of CCFA comply with the standard limits.

(2) The heat of hydration displays a declining trend with an increase in fly ash blending. Although there are differences in the early heat release rate between CFA and CCFA samples, the final cumulative heat release demonstrates substantial similarity.

(3) All mortars containing blended fly ash had PEC < 0 at 3 days; CFA and CCFA behaved as inert fillers at this stage. After 180 days of hydration, all fly ash-blended samples exhibited considerable pozzolanic activity (PEC > 0.5). Incorporating CCFA into the cement improved the long-term mechanical properties.

(4) At 180 d, both CFA and CCFA samples produced the secondary hydration product, C-A-S-H. The consumption of CH by two kinds of fly ash is comparable, demonstrating that CCFA and CFA have similar pozzolanic activity.

Author Contributions: Conceptualization, writing—review and editing, X.D.; methodology, writing—original draft, H.D.; formal analysis, investigation, E.W.; formal analysis, investigation, P.Y.; writing—review and editing, supervision, Y.L. (Yongqiang Li); data curation, visualization, investigation, Y.L. (Yaoming Luo); funding acquisition, writing—review and editing, W.L. All authors have read and agreed to the published version of the manuscript.

Data Availability Statement: The data presented in this study are available on request.

Conflicts of Interest: The authors declare no conflicts of interest.

References

1. Zhang, S.; Wang, F.; Mei, Z.; Lv, L.; Chi, Y. Status and development of sludge incineration in China. *Waste Biomass Valorization* **2021**, *12*, 3541–3574. [CrossRef]
2. Jin, L.; Zhang, G.; Tian, H. Current state of sewage treatment in China. *Water Res.* **2014**, *66*, 85–98. [CrossRef]
3. Global and Chinese Sludge Treatment and Disposal Industry Development Research Report 2018. Available online: http://www.gepresearch.com/77/view-767588-1.html (accessed on 21 January 2019).
4. Sludge Treatment Discharge Should Develop in the Direction of Green and Low Carbon. 2022. Available online: http://epaper.cenews.com.cn/html/2022-07/12/content_78019.htm (accessed on 12 July 2022).
5. Disposal of Factory Sludge from Water Purification Plants in Shenzhen. 2022. Available online: http://swj.sz.gov.cn/sjfb/psglxgtjsj/content/post_10510005.html (accessed on 28 March 2023).
6. Yu, Q.; Lei, H.; Li, Z.; Li, H.; Chen, K.; Zhang, X.; Liang, R. Physical and chemical properties of waste-activated sludge after microwave treatment. *Water Res.* **2010**, *44*, 2841–2849. [CrossRef] [PubMed]
7. Wahaab, R.A.; Mahmoud, M.; van Lier, J.B. Toward achieving sustainable management of municipal wastewater sludge in Egypt: The current status and future prospective. *Renew. Sustain. Energy Rev.* **2020**, *127*, 109880. [CrossRef]
8. Meer, I.; Nazir, R. Removal techniques for heavy metals from fly ash. *J. Mater. Cycles Waste Manag.* **2017**, *20*, 703–722. [CrossRef]
9. Jambhulkar, H.P.; Shaikh, S.M.S.; Kumar, M.S. Fly ash toxicity, emerging issues and possible implications for its exploitation in agriculture; Indian scenario: A review. *Chemosphere* **2018**, *213*, 333–344. [CrossRef]
10. Stelmach, S.; Wasielewski, R. Co-combustion of dried sewage sludge and coal in a pulverized coal boiler. *J. Mater. Cycles Waste Manag.* **2008**, *10*, 110–115. [CrossRef]
11. Tang, Y.; Pan, J.; Li, B.; Zhao, S.; Zhang, L. Residual and ecological risk assessment of heavy metals in fly ash from co-combustion of excess sludge and coal. *Sci. Rep.* **2021**, *11*, 2499. [CrossRef]
12. Chen, J.; Sun, Y.; Zhang, Z. Evolution of trace elements and polluting gases toward clean co-combustion of coal and sewage sludge. *Fuel* **2020**, *280*, 118685. [CrossRef]

13. Zhang, G.; Hai, J.; Ren, M.; Zhang, S.; Cheng, J.; Yang, Z. Emission, mass balance, and distribution characteristics of PCDD/Fs and heavy metals during cocombustion of sewage sludge and coal in power plants. *Environ. Sci. Technol.* **2013**, *47*, 2123–2130. [CrossRef]

14. Sarabèr, A.J. Co-combustion and its impact on fly ash quality; full-scale experiments. *Fuel Process. Technol.* **2014**, *128*, 68–82. [CrossRef]

15. Danish, A.; Ozbakkaloglu, T. Greener cementitious composites incorporating sewage sludge ash as cement replacement: A review of progress, potentials, and future prospects. *J. Clean. Prod.* **2022**, *371*, 133364. [CrossRef]

16. Murakami, T.; Suzuki, Y.; Nagasawa, H.; Yamamoto, T.; Koseki, T.; Hirose, H.; Okamoto, S. Combustion characteristics of sewage sludge in an incineration plant for energy recovery. *Fuel Process. Technol.* **2009**, *90*, 778–783. [CrossRef]

17. *DB 31/1291-2021*; Emission Standard of Air Pollutants for Coal and Sludge Co-Fired Power Plant. Shanghai Municipal Bureau of Ecology and Environment: Shanghai, China, 2021.

18. Li, J.S.; Xue, Q.; Fang, L.; Poon, C.S. Characteristics and metal leachability of incinerated sewage sludge ash and air pollution control residues from Hong Kong evaluated by different methods. *Waste Manag.* **2017**, *64*, 161–170. [CrossRef] [PubMed]

19. Lynn, C.J.; Dhir, R.K.; Ghataora, G.S. Environmental impacts of sewage sludge ash in construction: Leaching assessment, Resources. *Conserv. Recycl.* **2018**, *136*, 306–314. [CrossRef]

20. Wu, Z.; Jiang, Y.; Guo, W.; Jin, J.; Wu, M.; Shen, D.; Long, Y. The long-term performance of concrete amended with municipal sewage sludge incineration ash. *Environ. Technol. Innov.* **2021**, *23*, 101574. [CrossRef]

21. Nilimaa, J. Smart materials and technologies for sustainable concrete construction. *Dev. Built Environ.* **2023**, *15*, 100177. [CrossRef]

22. Zhang, L.; Ito, M.; Sato, A.; Ninomiya, Y.; Sakano, T.; Kanaoka, C.; Masui, M. Combustibility of dried sewage sludge and its mineral transformation at different oxygen content in drop tube furnace. *Fuel Process. Technol.* **2004**, *85*, 983–1011. [CrossRef]

23. Sarabèr, A. Co-combustion and its impact on fly ash quality; pilot-scale experiments. *Fuel Process. Technol.* **2012**, *104*, 105–114. [CrossRef]

24. Kijo-Kleczkowska, A.; Środa, K.; Kosowska-Golachowska, M.; Musiał, T.; Wolski, K. Experimental research of sewage sludge with coal and biomass co-combustion, in pellet form. *Waste Manag.* **2016**, *53*, 165–181. [CrossRef]

25. Kijo-Kleczkowska, A.; Środa, K.; Kosowska-Golachowska, M.; Musiał, T.; Wolski, K. Combustion of pelleted sewage sludge with reference to coal and biomass. *Fuel* **2016**, *170*, 141–160. [CrossRef]

26. Gao, F.; Zhou, C.; Du, J.; Zhang, Y.; Wu, W.; Liu, G.; Li, D. Effect of gaseous agents on co-combustion characteristics of sewage sludge and coal. *J. Environ. Chem. Eng.* **2021**, *9*, 106227. [CrossRef]

27. Ma, M.; Liang, Y.; Xu, D.; Sun, S.; Zhao, J.; Wang, S. Gas emission characteristics of sewage sludge co-combustion with coal: Effect of oxygen atmosphere and feedstock mixing ratio. *Fuel* **2022**, *322*, 124102. [CrossRef]

28. Xu, T.; Wang, C.; Hong, D.; Li, S.; Yue, S. The synergistic effect during co-combustion of municipal sludge and coal: Experimental and ReaxFF molecular dynamic study. *Energy* **2023**, *262*, 125553. [CrossRef]

29. Stasta, P.; Boran, J.; Bebar, L.; Stehlik, P.; Oral, J. Thermal processing of sewage sludge. *Appl. Therm. Eng.* **2006**, *26*, 1420–1426. [CrossRef]

30. Rao, M.; Ye, J.; Chen, C.; Kuang, C.; Chen, G.; Zou, X.; Qin, S.; Chen, L.; Liang, S. Construction of iterative algorithm and economic optimization analysis of co-combustion of sewage sludge with coal. *Int. J. Green Energy* **2022**, *20*, 925–933. [CrossRef]

31. Tan, P.; Ma, L.; Xia, J.; Fang, Q.; Zhang, C.; Chen, G. Co-firing sludge in a pulverized coal-fired utility boiler: Combustion characteristics and economic impacts. *Energy* **2017**, *119*, 392–399. [CrossRef]

32. Tong, C. *Study on the Formation Mechanism and Control Technology of Dioxins in the Process of Municipal Solid Waste Incineration*; Zhejiang University: Zhejiang, China, 2006.

33. Huang, H.; Buekens, A. On the mechanisms of dioxin formation in combustion processes. *Chemosphere* **1995**, *31*, 4099–4117. [CrossRef]

34. Nadziakiewicz, J.; Kozioł, M. Co-combustion of sludge with coal. *Appl. Energy* **2003**, *75*, 239–248. [CrossRef]

35. Cenni, R.; Janisch, B.; Spliethoff, H.; Hein, K. Legislative and environmental issues on the use of ash from coal and municipal sewage sludge co-firing as construction material. *Waste Manag.* **2001**, *21*, 17–31. [CrossRef]

36. Al-Ayish, N.; During, O.; Malaga, K.; Silva, N.; Gudmundsson, K. The influence of supplementary cementitious materials on climate impact of concrete bridges exposed to chlorides. *Constr. Build. Mater.* **2018**, *188*, 391–398. [CrossRef]

37. Cretescu, I.; Harja, M.; Teodosiu, C.; Isopescu, D.N.; Chok, M.F.; Sluser, B.M.; Salleh, M.A.M. Synthesis and characterisation of a binder cement replacement based on alkali activation of fly ash waste. *Process Saf. Environ. Prot.* **2018**, *119*, 23–35. [CrossRef]

38. Tan, H.; Nie, K.; He, X.; Deng, X.; Zhang, X.; Su, Y.; Yang, J. Compressive strength and hydration of high-volume wet-grinded coal fly ash cementitious materials. *Constr. Build. Mater.* **2019**, *206*, 248–260. [CrossRef]

39. Goñi, S.; Guerrero, A.; Luxán, M.P.; Macías, A. Activation of the fly ash pozzolanic reaction by hydrothermal conditions. *Cem. Concr. Res.* **2003**, *33*, 1399–1405. [CrossRef]

40. *GB 8076-2008*; Concrete Admixtures. Standards Press of China: Beijing, China, 2008.

41. Schöler, A.; Lothenbach, B.; Winnefeld, F.; Zajac, M. Hydration of quaternary Portland cement blends containing blast-furnace slag, siliceous fly ash and limestone powder. *Cem. Concr. Compos.* **2015**, *55*, 374–382. [CrossRef]

42. *GB/T 17671-2021*; Test Method of Cement Mortar Strength (ISO Method). Standards Press of China: Beijing, China, 2021.

43. Záleská, M.; Pavlíková, M.; Pavlík, Z.; Jankovský, O.; Pokorný, J.; Tydlitát, V.; Svora, P.; Černý, R. Physical and chemical characterization of technogenic pozzolans for the application in blended cements. *Constr. Build. Mater.* **2018**, *160*, 106–116. [CrossRef]
44. Piasta, W.; Lukawska, M. The effect of sewage sludge ash on properties of cement composites. *Procedia Eng.* **2016**, *161*, 1018–1024. [CrossRef]
45. *GB/T 1596-2017*; Fly Ash Used for Cement and Concrete. Standards Press of China: Beijing, China, 2017.
46. Qian, J. *Fly Ash Properties and Fly Ash Concrete*; Science Press: Beijing, China, 2000. (In Chinese)
47. Taylor, H.F.W. *Cement Chemistry*; Thomas Telford: London, UK, 1997.
48. Jansen, D.; Neunhoeffer, F.G.; Lothenbach, B.; Neubauer, J. The early hydration of ordinary Portland cement (OPC): An approach comparing measured heat flow with calculated heat flow from QXRD. *Cem. Concr. Res.* **2012**, *42*, 134–138. [CrossRef]
49. Bensted, J. Some applications of conduction calorimetry to cement hydration. *Adv. Cem. Res.* **1987**, *1*, 35–44. [CrossRef]
50. Langan, B.W.; Weng, K.; Ward, M.A. Effect of silica fume and fly ash on heat of hydration of Portland cement. *Cem. Concr. Res.* **2002**, *32*, 1045–1051. [CrossRef]
51. Snelson, D.G.; Wild, S.; O'Farrell, M. Heat of hydration of Portland Cement–Metakaolin–Fly ash (PC–MK–PFA) blends. *Cem. Concr. Res.* **2008**, *38*, 832–840. [CrossRef]
52. Tkaczewska, E.; Małolepszy, J. Hydration of coal–biomass fly ash cement. *Constr. Build. Mater.* **2009**, *23*, 2694–2700. [CrossRef]
53. Kaminskas, R.; Cesnauskas, V.; Kubiliute, R. Influence of different artificial additives on Portland cement hydration and hardening. *Constr. Build. Mater.* **2015**, *95*, 537–544. [CrossRef]
54. Deschner, F.; Winnefeld, F.; Lothenbach, B.; Seufert, S.; Schwesig, P.; Dittrich, S.; Goetz-Neunhoeffer, F.; Neubauer, J. Hydration of Portland cement with high replacement by siliceous fly ash. *Cem. Concr. Res.* **2012**, *42*, 1389–1400. [CrossRef]
55. Fořt, J.; Šál, J.; Ševčík, R.; Doleželová, M.; Keppert, M.; Jerman, M.; Záleská, M.; Stehel, V.; Černý, R. Biomass fly ash as an alternative to coal fly ash in blended cements: Functional aspects. *Constr. Build. Mater.* **2021**, *271*, 121544. [CrossRef]
56. El Fami, N.; Ez-zaki, H.; Sassi, O.; Boukhari, A.; Diouri, A. Rheology, calorimetry and electrical conductivity related-properties for monitoring the dissolution and precipitation process of cement-fly ash mixtures. *Powder Technol.* **2022**, *411*, 117937. [CrossRef]
57. Nilimaa, J.; Hösthagen, A.; Emborg, M. Thermal crack risk of concrete structures: Evaluation of theoretical models for tunnels and bridges. *Nord. Concr. Res.* **2017**, *56*, 55–69.
58. Papadakis, V.G. Effect of fly ash on Portland cement systems. *Cem. Concr. Res.* **1999**, *29*, 1727–1736. [CrossRef]
59. Ram, S.; Tare, M.S.; Aswath, P.B.; Ralegaonkar, R.V. Potential of co-fired fly ashes as a construction material—A review. *Encycl. Renew. Sustain. Mater.* **2020**, *1*, 674–685.
60. Kamali, M.; Ghahremaninezhad, A. Effect of glass powders on the mechanical and durability properties of cementitious materials. *Constr. Build. Mater.* **2015**, *98*, 407–416. [CrossRef]
61. Cho, Y.K.; Jung, S.H.; Choi, Y.C. Effects of chemical composition of fly ash on compressive strength of fly ash cement mortar. *Constr. Build. Mater.* **2019**, *204*, 255–264. [CrossRef]
62. Geng, Z.; Tang, S.; Wang, Y.; He, Z.; Wu, K.; Wang, L. Stress relaxation properties of calcium silicate hydrate: A molecular dynamics study. *J. Zhejiang Univ. -SCIENCE A* **2024**, *25*, 97–115. [CrossRef]
63. Tang, S.; Wang, Y.; Geng, Z.; Xu, X.; Yu, W.; Chen, J. Structure, fractality, mechanics and durability of calcium silicate hydrates. *Fractal Fract.* **2021**, *5*, 47. [CrossRef]
64. Tang, S.; Hubao, A.; Chen, J.; Yu, W.; Yu, P.; Chen, E.; Deng, H.; He, Z. The interactions between water molecules and CSH surfaces in loads-induced nanopores: A molecular dynamics study. *Appl. Surf. Sci.* **2019**, *496*, 143744. [CrossRef]
65. Rossen, J.E.; Scrivener, K.L. Optimization of SEM-EDS to determine the C–A–S–H composition in matured cement paste samples. *Mater. Charact.* **2017**, *123*, 294–306. [CrossRef]
66. Rodger, S.A.; Groves, G.W. The microstructure of tricalcium silicate/pulverized-fuel ash blended cement pastes. *Adv. Cem. Res.* **1988**, *1*, 84–91. [CrossRef]
67. Zhang, Z.; Angst, U. Microstructure and moisture transport in carbonated cement-based materials incorporating cellulose nanofibrils. *Cem. Concr. Res.* **2022**, *162*, 106990. [CrossRef]
68. Lin, X.; Mao, T.; Chen, Z.; Chen, J.; Zhang, S.; Li, X.; Yan, J. Thermal cotreatment of municipal solid waste incineration fly ash with sewage sludge: Phases transformation, kinetics and fusion characteristics, and heavy metals solidification. *J. Clean. Prod.* **2021**, *317*, 128429. [CrossRef]
69. Ogawa, K.; Uchikawa, H.; Takemoto, K.; Yasui, I. The mechanism of the hydration in the system C3S-pozzolana. *Cem. Concr. Res.* **1980**, *10*, 683–696. [CrossRef]
70. Park, B.; Choi, Y.C. Hydration and pore-structure characteristics of high-volume fly ash cement pastes. *Constr. Build. Mater.* **2021**, *278*, 122390. [CrossRef]